Available online at www.sciencedirect.com

SciVerse ScienceDirect

Journal of the European Ceramic Society 32 (2012) 2487–2494

www.elsevier.com/locate/jeurceramsoc

Light transmittance in α-SiAlON ceramics: Effects of composition, microstructure, and refractive index anisotropy

Limeng Liu [a,b,*], Feng Ye [a], Siwei Zheng [a], Bo Peng [a], Wei Luo [a], Zhiguo Zhang [b], Yu Zhou [a]

[a] School of Materials Science and Engineering, Harbin Institute of Technology, Harbin 150001, China
[b] Department of Physics, Harbin Institute of Technology, Harbin 150001, China

Received 22 November 2011; received in revised form 15 February 2012; accepted 17 February 2012
Available online 13 March 2012

Abstract

Translucent α-SiAlON ceramics were synthesized by hot pressing and spark plasma sintering. The in-line transmittance of the visible-infrared light through the α-SiAlON ceramics was discussed in correlation with the SiAlON compositions, rare earth dopant types, microstructures, and the refractive index anisotropy of the α-SiAlON grains. The results showed that the α-SiAlON ceramics had a refractive index about 2.17 and a refractive index anisotropy about 0.014. The birefringent losses due to the index anisotropy were the main reason for the severe transmission degradation in the visible light regions in the transmission curves. Accordingly, smaller grain sizes could be used to counteract the large birefringent losses to improve the in-line transmittance of the short wavelength light.

Keywords: D. SiAlON; B. Microstructure-final; C. Optical properties; B. Grain size; E. Cutting tools

1. Introduction

The new generation of high-speed turning tools requires monitoring the real-time local temperatures of the cutting edges.[1] One feasible option is to use transparent ceramic tools, in which an infrared temperature detector is inserted. α-SiAlON and transparent Al_2O_3 ceramics are of high potential for such advanced tool applications.

The α-SiAlON is the solid-solution based on the α-Si_3N_4.[2,3] During the α-SiAlON formation, the Al–O and Al–N partly substitute for the Si–N, with some RE^{v+} cations (RE = Li, Ca, Y, and most rare earths except Pr, Tm, and Eu) being incorporated into the SiAlON lattice to balance the charge discrepancy. In the α-SiAlON general formula of $RE_{m/v}Si_{12-(m+n)}Al_{m+n}O_nN_{16-n}$, the m, n values can change in a relatively wide range without altering the α-SiAlON lattice structure. The microstructures, i.e. the grain sizes and the intergranular phase concentrations, of the α-SiAlON ceramics are significantly affected by the m, n values, the RE types, and the sintering conditions.

The α-SiAlON ceramics have hardness, fracture toughness, flexure strength, thermal shock resistance, and wear resistance much better than that of the Al_2O_3 ceramics.[4,5] Therefore α-SiAlONs are more suitable for cutting tool applications than the Al_2O_3.[6–8] The only one disadvantage of the α-SiAlON ceramics is the inferior light transmission. The α-SiAlON ceramics exhibit an in-line transmittance up to 72% in the middle infrared, but drastically decrease in the short wavelength region.[9–11] The insufficient in-line transmittance of the visible light always makes α-SiAlON ceramics opaque. In the few publications on the light transmittance of the α-SiAlON ceramics, the intergranular phases and the inhomogeneous microstructures (rather than the α-SiAlON grain sizes) were thought to be the reason for the insufficient light transmittance of the α-SiAlON ceramics. But no solidified rationales were offered to support those arguments.

It is known that the reflection losses by the front and back surfaces R_s and the theoretical (i.e. total) light transmission through an ideal optical medium T_{th} is dependent on the refractive index n of the optical medium by Eqs. (1) and (2), respectively. In another word, the inferior light transmission of the α-SiAlON ceramics in comparison

* Corresponding author at: School of Materials Science and Engineering, Harbin Institute of Technology, Harbin 150001, China. Tel.: +86 451 86413921; fax: +86 451 86413922.
E-mail address: liulimeng@hit.edu.cn (L. Liu).

0955-2219/$ – see front matter © 2012 Elsevier Ltd. All rights reserved.
doi:10.1016/j.jeurceramsoc.2012.02.027

Table 1
Composition, microstructural and optical characteristics of the α-SiAlON ceramics.

Materials	α-SiAlON composition	Sintering additive	Intergranular phase content (%)	Grain size r (μm)	Calculated by ln(*RIT*)-*d*		Refined by simulation		Experimentally measured
					n	Δn	n	Δn	n
HP-Dy1010	$Dy_{1/3}Si_{10}Al_2ON_{15}$	2 wt% Dy_2O_3	3.4	0.493	2.16	0.008	Not done	Not done	2.11
HP-Y1510	$Y_{0.5}Si_{9.5}Al_{2.5}ON_{15}$	2 wt% Y_2O_3	4.2	0.429	2.15	0.011	2.04	0.0110	2.17
SPS-Y1510	$Y_{0.5}Si_{9.5}Al_{2.5}ON_{15}$	2 wt% Y_2O_3	4.9	1.099	2.15	0.013	2.04	0.0136	2.13
HP-YbY1010	$Yb_{1/6}Y_{1/6}Si_{10}Al_2ON_{15}$	2 wt% $YbYO_3$	3.7	0.553	Not done	Not done	1.96	0.0060	2.05
HP-YbNd1010	$Yb_{1/6}Nd_{1/6}Si_{10}Al_2ON_{15}$	2 wt% $YbNdO_3$	3.2	0.523	Not done	Not done	2.08	0.0045	2.12

with Al_2O_3 could be dictated by the index n of the α-SiAlON.

$$R_s = \frac{(n-1)^2}{n^2+1} \quad (1)$$

$$T_{th} = \frac{2n}{n^2+1} \quad (2)$$

On the other hand, the α-SiAlON ceramics usually consist of a small amount of intergranular phases besides the α-SiAlON grains, both introduce optical anisotropy to the α-SiAlON ceramics due to the asymmetry of the individual α-SiAlON grains and the refractive index differences between the α-SiAlON grain and the intergranular phase. Accordingly, the quality of light transmission is determined by the in-line transmission (*RIT*) rather than the total value. This transmission difference is expected because the light beam is refracted by the individual SiAlON grains and also reflected at the interfaces between two neighboring grains, thus disturb the light beam.

Light transmission theory predicts the *RIT* of a polycrystalline optically anisotropic material[12] by equation (3).

$$RIT = T_{th} \exp\left\{\frac{-3\pi^2 \Delta n^2 rd}{n^2 \lambda^2}\right\} \quad (3)$$

where n is the refractive index of the material (in case of an α-SiAlON ceramic, n is the average of the α-SiAlON grains and the intergranular phases); Δn is the refractive index difference (also averaged considering both the α-SiAlON grains and the intergranular phases), the grain size $2r$, wavelength in vacuum λ, and sample thickness d.

Eq. (3) indicates that *RIT* is determined by both the intrinsic optical parameters and the microstructural factors. To our knowledge, there are no reports on the optical parameters, such as refractive index n and refractive index difference Δn of the α-SiAlON ceramics, making the arguments on the light transmission of the α-SiAlON ceramics less cogent.

In this study, translucent α-SiAlON ceramics were synthesized by hot pressing and spark plasma sintering. The microstructures of the α-SiAlON ceramics were changed by varying the compositions, the rare earth types and the sintering conditions. The refractive indices were determined by the Abbé measurement. The refractive index difference, as the indicator of the birefringent loss shown in Eq. (3), was determined by computational simulation of the transmission lines according to Eq. (3). The feasible way to improve the visible-infrared light transmittances through the α-SiAlON ceramics was discussed.

2. Experimental

The investigated compositions of the α-SiAlON ceramics are listed in Table 1. The compositions were located in the single phase α-SiAlON area, thus should yield pure α-SiAlON at complete phase formation. Two weight percents rare earth oxides were used as the sintering aids. Considering the different molecular weights of the rare-earth oxides (i.e. 394.08 for Yb_2O_3, 336.48 for Nd_2O_3, and 223.19 for Y_2O_3) the 2% in weight addition meant more sintering additives in the Y-containing SiAlONs than the Yb- and/or Nd-containing counterparts. This may results in more inter granular phase in the Y-SiAlON samples. High-purity powders of Si_3N_4 (E10 Grade, UBE Industries Ltd., Japan), AlN (Grade F, Tokuyama Corp., Japan), Al_2O_3 (AKP-50, Sumitomo Chemical, Japan), Dy_2O_3, Nd_2O_3, and Y_2O_3 (>99.9% purity, Shinetsu Chemical Co., Ltd., Japan) were used as the starting materials. The powder mixtures in proper proportions were homogenized in a plastic bottle containing ethanol and silicon nitride balls for 8 h. The slurries were dried and passed through a 120 mesh sieve.

Hot pressing (HP) and spark plasma sintering (SPS) were applied to densify the materials. Batches of the powder mixture were cold pressed under 10–15 MPa uniaxial pressure to produce the green compacts. The green compacts were set in the HP/SPS die for sintering. The HP/SPS die was lined by a thick BN layer to prevent the α-SiAlON samples from being contaminated by carbon. The hot pressing was performed at 1900 °C for 1 h under 32 MPa pressure in 0.4 MPa nitrogen, using heating and cooling rate of 20 °C/min. The SPS process was performed at 1800 °C for 10 min under 30 MPa in 0.1 MPa nitrogen, with heating and cooling rate of 100 °C/min and 300 °C/min respectively. The designations of the α-SiAlON ceramics are shown in Table 1, referring both the α-SiAlON compositions and the sintering conditions. For example, the HP-Dy1010 was the α-SiAlON with a composition $m = 1.0$, $n = 1.0$ in the general formula of $RE_{m/v}Si_{12-(m+n)}Al_{m+n}O_nN_{16-n}$, and hot pressed at 1900 °C for 1 h.

The as-sintered materials were sectioned, ground and polished to 1 μm diamond finish. Densities were measured by the Archimedes method. The phase assemblages were characterized by X-ray diffractometry (XRD). Transmission electron microscopy (TEM, CM-12, the Netherlands) with an energy

dispersive X-ray spectroscope attachment (EDXS) was used to detail the microstructures. The contents of the intergranular phases were calculated by counting their areas in the TEM micrographs using an Image-Pro Plus software compact (Media Cybernetics, Inc., MD, USA). The α-SiAlON grain morphologies were observed by scanning electron microscopy (SEM, Hitachi S-3500N, Japan), after etching the samples in molten NaOH for 2–5 min.

The in-line transmittances from 200 to 3000 nm were measured by a Lumbda-950 UV-Visible-IR spectrophotometer (PerkinElmer, Inc., CA, USA). Only the light within the scattering angle of 0.5° was collected. The reflections on the front surfaces were recorded. The refractive indices of the different α-SiAlON materials were determined by two routines separately; Interphako interference microscopy was used to measure the refractive indices in a S-Se solid solution as the immerging medium. This S-Se medium could give a satisfactory measure of refractive indices up to 2.5. The other routine to calculate the refractive indices was based on Eq. (4) by replacing Eq. (3).

$$\ln(RIT) = \ln\ T_{\text{th}} - \frac{3\pi^2\Delta n^2 rd}{n^2\lambda^2} \quad (4)$$

According to Eq. (4), the ln(*RIT*) was plotted vs. the sample thickness *d* at different wavelength λ. Then the T_{th} can be calculated from the intercept at the *Y*-axis, and *n* be determined according to Eq. (2), Δ*n* determined by the slope of the ln(*RIT*)-*d* plot. Computational simulation of the transmission curves of the different α-SiAlON ceramics[12,13] was done according to Eq. (3) to check the validity of the measured and the calculated *n* and Δ*n* values.

3. Results

3.1. The α-SiAlON grain sizes and the intergranular phases

All the as-sintered samples reached their theoretical densities, indicating the efficiency of using the 2 wt% extra rare earth oxides as the sintering additives. The XRD patterns of the materials are shown in Fig. 1. α-SiAlON dominated the phase compositions. Very small concentrations of M′ phase were present in the HP-Y1510 and the SPS-Y1510 materials, whereas no crystalline secondary phases were detected in the other materials, possibly due to the extremely low contents or the glassy nature of the secondary phases. The relatively more molar ratios of the Y_2O_3, compared with the Yb_2O_3 and Nd_2O_3 additives to the SiAlONs explained the presence of the M′ in the Y-SiAlON ceramics.

Typical SEM and TEM micrographs of the α-SiAlON materials are shown in Fig. 2. Before the SEM observation, the boundary phases of the α-SiAlON ceramics were leached off by the molten NaOH to expose the individual grains as being observed in the SEM micrographs. Assuming the individual α-SiAlON grains as spheres, the equivalent diameter 2*r* were calculated,[12] and the 2*r* values are listed in Table 1. It can be seen the hot pressed materials generally had smaller grain sizes (with average radius less than 0.550 μm), compared to the spark plasma sintered SPS-Y1510 material (with average radius

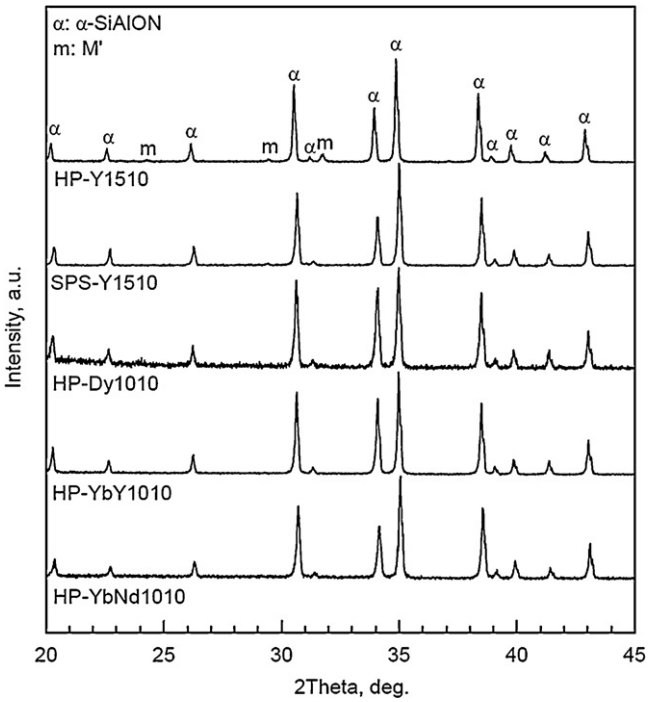

Fig. 1. The XRD patterns of the α-SiAlON ceramics, showing dominant α-SiAlON. Some M′ phase exists in HP-Y1510 and SPS-Y1510 materials.

1.099 μm). The fast heating rate of SPS should have yielded more transient RESiAlON liquid during the α-SiAlON phase formation process by preventing forming the various crystalline intermediate phases, thus favors the fast growth of the selected α-SiAlON nuclei, to result in the significantly enlarged α-SiAlON grains.

The TEM micrographs in Fig. 2 showed fully dense α-SiAlON. No residual pores were observed at any locations. Intergranular phases were presented at the triple conjunctions and also along the grain boundaries. The concentrations of the intergranular phases were calculated by image analysis and the results are listed in Table 1. It exhibited that the SPS-Y1510 material had the highest intergranular phase concentration up to 4.9% whereas the HP-YbNd1010 material had the lowest concentration of 3.2%. Selected-area electron diffraction (SAED) confirmed that the intergranular phases at some triple conjunctions in the HP-YbNd1010 and the SPS-Y1510 materials were partly crystallized as the M′ phase whereas the intergranular phases in the other materials were predominantly glassy.

Fig. 2 shows a large population of dislocations in the α-SiAlON grains of the SPS-Y1510 material. Higher local rare earth concentration in the center than in the rim of the individual α-SiAlON grains was expected, for the fast grain growth in SPS.[10]

3.2. Light transmittance

The transparency of the α-SiAlON ceramics was shown by the inserts in Fig. 2. The effects of the carbon contamination from the graphite HP/SPS die could be excluded due to the efficiency of lining the die by BN. The inserts in Fig. 2 showed the

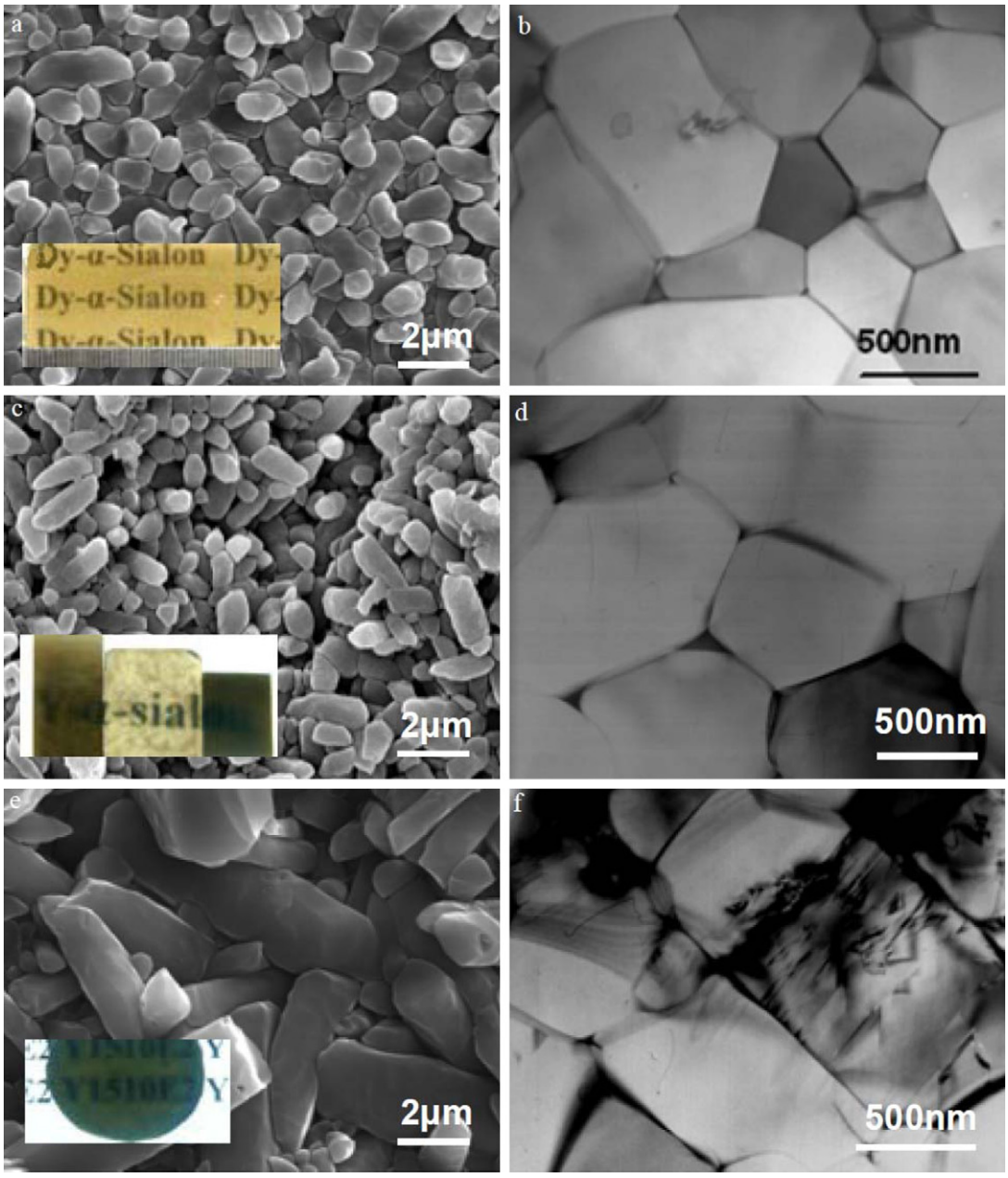

Fig. 2. The SEM and TEM micrographs of the HP-Dy1010 (a, b), HP-Y1510 (c, d), and SPS-Y1510 (e, f) materials. The inserts show the visible light transmittances of the Dy-SiAlON at 0.8 mm, HP-Y1510 (middle) and SPS-Y1510 materials at 1.0 mm thickness.

SPS-Y1510 material had poor transparency in comparison with the clear visible light transmission of the counterpart HP-Y1510 and other materials.

The typical transmission curves as a function of the sample thicknesses and the light wavelengths are shown in Figs. 3 and 4. All the α-SiAlON ceramics exhibited absorption limits and infrared cut off edges at about 340 nm and 6500 nm, due to the charge transfer and the 2.0–2.5 eV optical energy gap, respectively. In the wavelength range of 340–3000 nm, the transmittances of the different α-SiAlON samples increased exponentially with the wavelength. The Wien's displacement law of $\lambda_m T = 2.898 \times 10^{-3}$ m K, predicated 1900–2300 nm emission at 900–1200 °C which is corresponding with the permissive application temperature range for α-SiAlON ceramics. Therefore, the fairly good transmittance at 1900–2300 nm as shown in Figs. 3 and 4 indicated potential of the α-SiAlON ceramics for transparent cutting tool applications.

The various strong absorption peaks in the transmission curves of Figs. 3 and 4 were caused by the f→f and 5d→4f electron transition[3] of the Dy^{3+}, Yb^{3+} and Nd^{3+} ions. The Y^{3+} did not have such electron transmissions, therefore no absorption peaks in the SPS-Y1510 and HP-Y1510 materials.

3.3. The refractive index and the optical anisotropy of the α-SiAlON samples

The refractive indices of the α-SiAlON samples measured by the interphako interference microscopy are listed in Table 1.

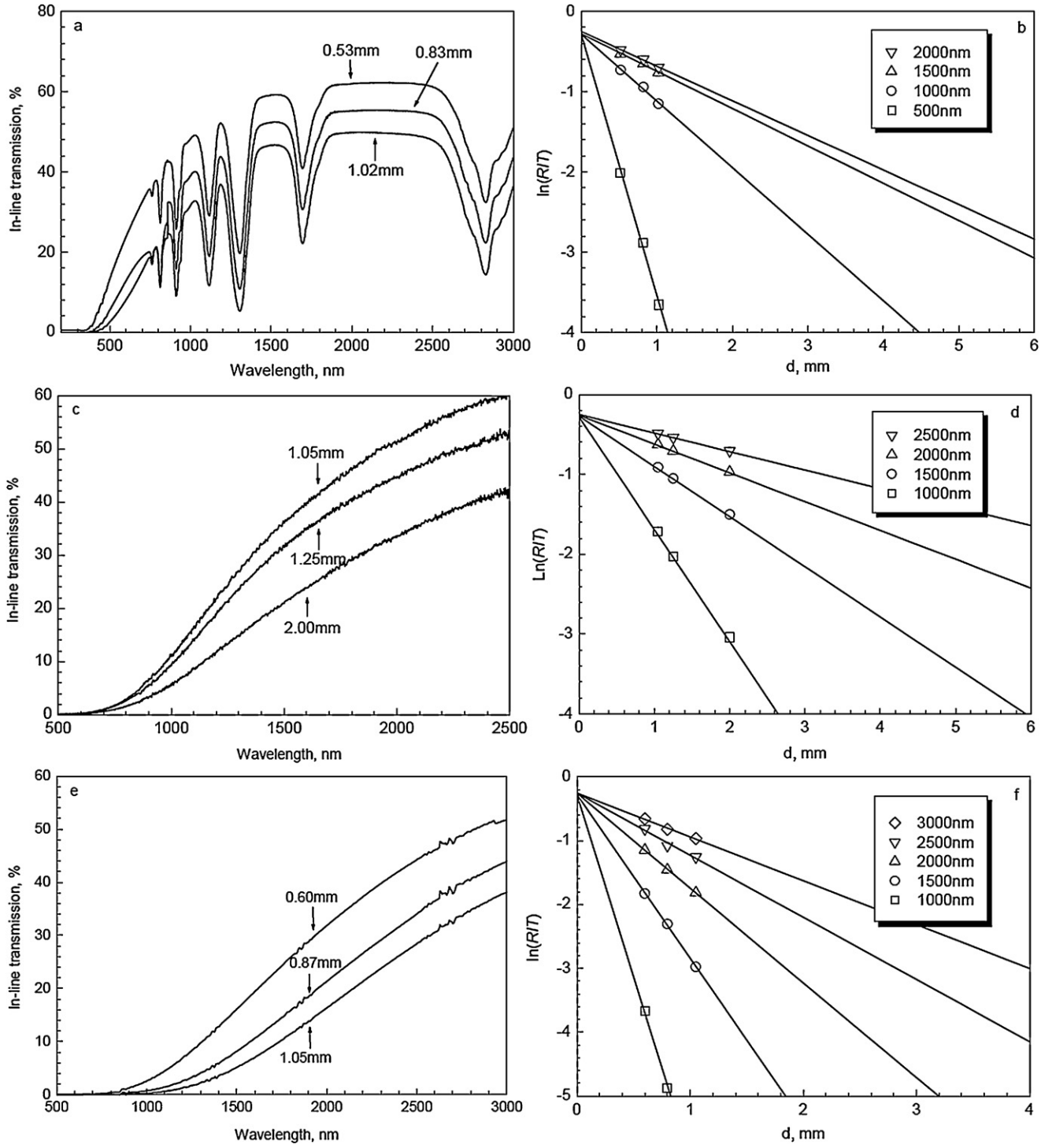

Fig. 3. The in-line transmittance of the α-SiAlON ceramics at different thicknesses, and the ln(*RIT*)-*d* plots for the (a, b) HP-Dy1010, (c, d) HP-Y1510, and (e, f) SPS-Y1510 materials.

It can be seen the different α-SiAlON materials had refractive indices in the range of 2.05–2.17, which were very similar, regardless the different rare earth dopants, the slightly different phase compositions and the different microstructures as detailed in the prior section.

The ln(*RIT*)-*d* plots for the selected wavelengths are shown in Fig. 3. Linear relationships were satisfied. The refractive indices n and the index differences Δn were calculated by the y-intercept, the slope of that line, the grain diameter $2r$, as mentioned in the introduction. The calculated results showed the α-SiAlON samples had slightly higher refractive index at the shorter wavelengths in the concerned ranges.[1] For example, the HP-Dy1010 material exhibited refractive index of 2.08 and 2.21 at 2000 nm and 500 nm, respectively. Thus the calculated indices n at different wavelengths were averaged and the average values are reported in Table 1.

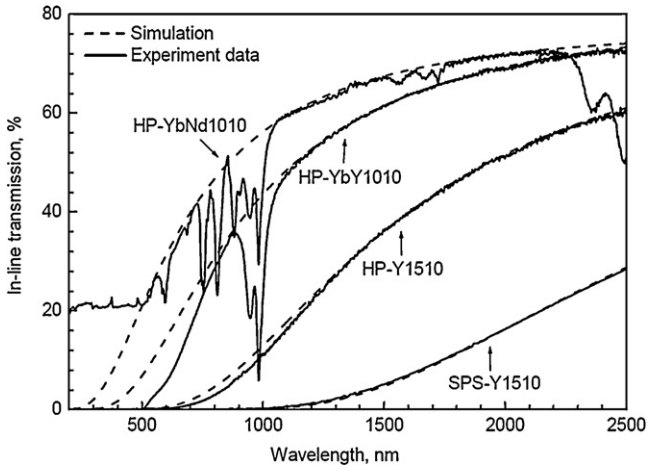

Fig. 4. Simulation of the in-line transmission of α-SiAlON ceramics at 1.0 mm thick, perfectly matching the experimental results. The HP-YbNd1010 material shows better UV–vis transmission.

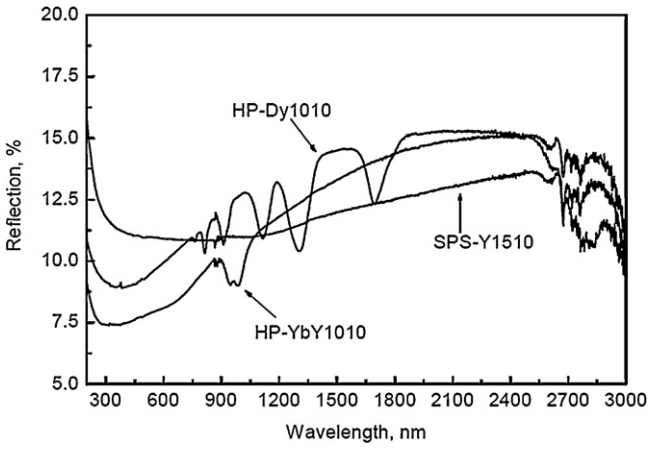

Fig. 5. Diffuse reflection curve of the normal incidence light from the front surfaces of the different α-SiAlON materials.

The index differences Δn of the different α-SiAlON samples fell in the range of 0.008–0.013, independent of the wavelength,[14] but strongly affected by the sintering methods, the rare earth dopants, and the microstructures. The compositional inhomogeneity and the high dislocation concentrations in the SPS-Y1510 material (see Fig. 2f) presumably explained the higher Δn for the SPS-Y1510. The intergranular phase concentration may also increase the refractive index anisotropy, i.e. larger Δn, of the α-SiAlON ceramics. However, considering the extremely small concentrations of the intergranular phases in the different α-SiAlON samples, the Δn values could be predominantly attributed to the crystallographic anisotropy of the hexagonal α-SiAlON grains. The refractive index differences between the intergranular phases and the α-SiAlON grains should also contribute to part of the Δn for an α-SiAlON ceramic.

The in-line transmission curves were computationally simulated using Eq. (3) to verify the measured/calculated n and Δn. The best fit simulations are shown in Fig. 4 by the dash lines and the best fit refractive indices n and the index differences Δn are listed in Table 1. The good agreement between the experimentally measured, the calculated and the simulated values indicated the validity of the n and Δn.

According to the experimentally measured values of n, the reflections on the front surfaces of the different materials were estimated ∼13.3% (the combination form both front and back surfaces was up to 23.5%). Fig. 5 shows the typical light reflections from the front surfaces of the HP-Dy1010, HP-YbY1010, and the SPS-Y1510 materials at normal incidence of the light beam. The HP-Dy1010 and the HP-YbY1010 material exhibited similar reflections at 1800–2700 nm wavelength, if regardless the absorption edges. Good agreements between the predicated and the measured reflection values were observed in both materials. However, the SPS-Y1510 sample showed strangely lower reflection than the predication by n. This suggested a few percent of light being absorbed by the α-SiAlON bulk, the reason of which may be associated with the higher population of the dislocations in the α-SiAlON grains.

4. Discussion

Fully dense Y, Dy, YbY, and YbNd doped α-SiAlON ceramics with different compositions could be prepared by HP/SPS. The HP materials had finer microstructures with average grain sizes <0.550 μm, while the SPS-Y1510 material had a larger average grain size of ∼1.099 μm. The SPS-Y1510 sample also had a larger intergranular phase concentration and a higher dislocation population in the SPS α-SiAlON grains. These microstructural differences, however, showed relatively insignificant effects on the refractive indices and the refractive index anisotropy of the different materials. As listed in Table 1, the n and Δn values were around 2.10 and 0.010, respectively, in all of the materials.

In Table 1, the largest n value for the α-SiAlON ceramics (up to 2.17) is comparable to the refractive indices of c-ZrO_2[15] and single Si_3N_4 crystals, but higher than Al_2O_3 ($n = 1.76$) and YAG ($n = 1.84$).[16] The refractive indices of Si_3N_4 were reported in the range of 2.0–2.055.[17,18] Si_3N_4 fabricated by chemical vapor deposition had a higher refractive index of 2.055 at 470 nm.[18] Therefore, it seemed the RE^{3+}, $Al^{3+}$and O^{2-} incorporation into the Si_3N_4 lattice increased the refractive index of the α-SiAlON ceramics.

Based on the measured n values, the inferior *RIT* of the α-SiAlON ceramics than the transparent alumna was explained. The lower transmission of the α-SiAlON ceramics was partially attributed to the higher refractive index values. The theoretical transmission limit T_{th}, referring Eq. (2) and the a reasonable average refractive index of 2.15 in 500–2000 nm wavelength as shown in Table 1, was calculated to be ∼76.5%, intrinsically lower than the $T_{th} = 85.9\%$ for polycrystalline alumna with $n = 1.76$.

Figs. 3 and 4 showed the in-line transmittance degraded drastically with the decrease of the wavelength. This in-line transmission degradation was due to the optical anisotropy of the individual α-SiAlON grains and the refractive index difference between the α-SiAlON grains and the intergranular phases, the effects of which were summarized by the parameter Δn.

Eq. (3) predicated birefringent losses in an exponent way by the Δn and the large grain sizes. The in-line transmission would decrease with the increase of $\Delta n^2 \cdot r/\lambda^2$ at a given sample thickness, in good consistency with the in-line transmission shown in Figs. 3 and 4. For comparison, isotropic materials such as garnet and spinal with $\Delta n = 0$ demonstrated steady transmissions, irrelevant to wavelength and grain sizes.

Fig. 4 illustrates a sequence of the in-line transmission loss in the short wavelength region as SPS-Y1010 > HP-Y1010 > HP-YbY1010 > HP-YbNd1010, meanwhile $\Delta n^2 \cdot r$ values decreased from 0.203 to 0.011 nm. In Figs. 3 and 4, the SPS-Y1510 material gave no light transmittance at $\lambda = 640$ nm and $d = 1$ mm. In contrast, 40–50% transmission in the HP-YbY1010 and HP-YbNd1010 materials were presented. However, this 40–50% transmission was still lower than that of a dense Al_2O_3 ceramic (*RIT* up to 60–65% with comparable grain size), demonstrating the bad effects of the higher Δn values for α-SiAlONs in comparison with the Al_2O_3 ceramic ($\Delta n \sim 0.01$ in α-SiAlON vs. 0.005 in Al_2O_3).

The Apetz's model, i.e. the $RIT \sim \Delta n^2 \cdot r$ correlation expressed by Eq. (3) demonstrated that the birefringent scattering by the larger Δn could be compensated by smaller grain size. As shown in Fig. 4, in-line transmission of 61.1% and 38.1% at 2500 nm were obtained in the HP-Y1510 and SPS-Y1510 ceramic, respectively. Although both materials had similar n and Δn (Table 1), it was quite clear that the 2.56 folds smaller crystal size in the HP-Y1510 material gave a 23% higher transmission (Table 1). Su and colleagues[10] observed similar transmission decrease behavior in a Dy-doped α-SiAlON ceramics.

In summary, before we tried in this study to correlate the in-line transmission with the birefringent losses caused by larger n, Δn and coarse grains as discussed in the prior sections, previous literatures attributed the better transparency of the α-SiAlON ceramics to such reasons as glass-free grain boundaries, full density and uniform microstructures (rather than smaller α-SiAlON grain sizes).[6,9] The intergranular phases were once thought to be the primary reason for the transmission loss, may be partly true considering the possible different n and Δn from that of the α-SiAlON phase. However, in fact the existence of the intergranular phases as thin films along the boundaries should have relatively insignificant influence on the in-line transmission due to the small concentrations.

The light transmission physics suggested that elimination of the refractive index difference between the α-SiAlON grains and the intergranular phases would reduce birefringent losses at the interfaces, hence higher in-line light transmission. However, although the refractive indices for MSiAlON glass (M = Ca, Dy, Er, La, Nd, Sm, Y, Yb) were modulated in the wide range of 1.62–2.3 at 500–640 nm by the N and M contents,[19–21] it was technically impossible to completely match the intergranular phases with the α-SiAlON grains to eliminate in-line transmission loss, caused by the refractive index difference between the α-SiAlON grains and the surrounding intergranular phases.[15] However, as indicated by the discussions of this study, such a deleterious effect could be conveniently compensated by diminishing the sizes of the α-SiAlON grains by conveniently changing the compositions and sintering control techniques.

5. Conclusions

(1) The in-line visible-IR transmission through the α-SiAlON ceramics was dictated by the optical parameters of the refractive index n and the index difference Δn; and was also affected by the microstructural factors of the grain sizes and the intergranular phase concentrations.
(2) The refractive index n and index anisotropy Δn for the α-SiAlON ceramics were in the range of 2.05–2.17 and 0.0045–0.0136, respectively. They were insensitive to SiAlON compositions or the microstructures.
(3) The theoretical transmission limit was predicated to be ~76.5% for α-SiAlON ceramics. Smaller α-SiAlON grains could be used to increase the in-line transmission of the short wavelength light.

Acknowledgment

This work was financially supported by "The Fundamental Research Funds for the Central Universities" under Grant No. HIT. NSRIF 2010111.

References

1. Krell A, Hutzler T, Klimke J. Transmission physics and consequences for materials selection, manufacturing, and applications. *J Eur Ceram Soc* 2009;**29**:207–21.
2. Izhevskiy V, Genova L, Bressiani J, Aldinger F. Progress in SiAlON ceramics. *J Eur Ceram Soc* 2000;**20**:2275–95.
3. Shen Z, Nygren M, Halenius U. Absorption spectra of rare-earth-doped α-SiAlON ceramics. *J Mater Sci Lett* 1997;**16**:263–6.
4. Kim J, Rosenflanz A, Chen I-W. Microstructure control of in situ toughened α-SiAlON ceramics. *J Am Ceram Soc* 2000;**83**(7):1819–21.
5. Shuba R, Chen I-W. Effect of seeding on the microstructure and mechanical properties of α-SiAlON: II, Ca–SiAlON. *J Am Ceram Soc* 2001;**85**(5):1260–7.
6. Mandal H. New developments in α-SiAlON ceramics. *J Eur Ceram Soc* 1999;**19**:2349–57.
7. Chen I-W, Rosenflanz A. A tough SiAlON ceramic based on α-Si_3N_4 with a whisker-like microstructure. *Nature* 1997;**389**:701–4.
8. Pettersson P, Shen Z, Johnsson M, Nygren M. Thermal shock resistence of α/β-SiAlON ceramic composites. *J Eur Ceram Soc* 2001;**21**:999–1005.
9. Jones MI, Hyuga H, Hirao K, Yamauchi Y. Highly transparent Lu-α-SiAlON. *J Am Ceram Soc* 2004;**87**(4):714–6.
10. Su P, Wang W, Chen Y, Cheng, Yan D. Infrared transmission of tot-pressed Y- and Dy-α-sialon ceramics. *Mater Lett* 2004;**58**:1985–8.
11. Chen W, Su X, Wang P, Yan D. Optical properties of Gd-α-Sialon ceramics: effect of carbon contamination. *J Am Ceram Soc* 2005;**88**(8):2304–6.
12. Apetz R, Bruggen M. Transparent alumina: a light-scattering model. *J Am Ceram Soc* 2003;**86**(3):480–6.
13. Berthier T, Fokin VM, Zanotto ED. New large grain, highly crystalline, transparent glass-ceramics. *J Non-Cryst Solids* 2008;**354**:1721–30.
14. Thomas ME, Andersson SK, Sova RM, Joseph RI. Frequency and temperature dependence of the refractive index of sapphire. *Infrared Phys Technol* 1998;**39**(4):235–49.
15. Peuchert U, Okano Y, Menke Y, Reichel S, Ikesue A. Transparent cubic-ZrO_2 ceramics for application as optical lenses. *J Eur Ceram Soc* 2009;**29**:283–91.
16. Saikawa J, Sato Y, Taira T, Ikesue A. Absorption, emission spectrum properties, and efficient laser performances of Yb:$Y_3ScAl_4O_{12}$ ceramics. *Appl Phys Lett* 2004;**85**(11):1898–900.
17. Boyd JT, Kuo CS. Composite prism-grating coupler for coupling light into high refractive index thin-film waveguides. *Appl Opt* 1976;**15**:1681–3.

18. Yoon DH, Yoon SG, Kim YT. Refractive index and etched structure of silicon nitride waveguides fabricated by PECVD. *Thin Solid Films* 2007;**515**:5004–7.
19. Sharafat A, Grins J, Esmaeilzadeh S. Hardness and Refractive Index of Ca–Si–O–N Glasses. *J Non-Cryst Solids* 2009;**355**:301–4.
20. Hakeem AS, Grins J, Esmaeilzadeh S. La–Si–O–N glasses part II: vickers hardness and refractive index. *J Eur Ceram Soc* 2007;**27**:4783–7.
21. Redington W, Redington M, Hampshire S, Serantoni M. Properties of some high Al content glasses in various lanthanide–Si–Al–O–N systems. *J Non-Cryst Solids* 2003;**316**:74–81.